Humidity assay for studying plant-pathogen interactions in miniature controlled discrete humidity environments with good throughput

Zhen Xu, Huawei Jiang, Binod Bihari Sahu, Sekhar Kambakam, Prashant Singh, Xinran Wang, Qiugu Wang, Madan K. Bhattacharyya, and Liang Dong

Citation: Biomicrofluidics **10**, 034108 (2016); doi: 10.1063/1.4950998
View online: http://dx.doi.org/10.1063/1.4950998
View Table of Contents: http://scitation.aip.org/content/aip/journal/bmf/10/3?ver=pdfcov
Published by the AIP Publishing

Humidity assay for studying plant-pathogen interactions in miniature controlled discrete humidity environments with good throughput

Zhen Xu,[1] Huawei Jiang,[1] Binod Bihari Sahu,[2,3] Sekhar Kambakam,[2] Prashant Singh,[2,4] Xinran Wang,[1] Qiugu Wang,[1] Madan K. Bhattacharyya,[2] and Liang Dong[1,a)]

[1]*Department of Electrical and Computer Engineering, Iowa State University, Ames, Iowa 50011, USA*
[2]*Department of Agronomy, Iowa State University, Ames, Iowa 50011, USA*
[3]*National Institute of Technology, Rourkela, Odisha 769008, India*
[4]*Lancaster Environment Centre, Lancaster University, Lancaster LA1 4YQ, United Kingdom*

(Received 7 April 2016; accepted 9 May 2016; published online 18 May 2016)

This paper reports a highly economical and accessible approach to generate different discrete relative humidity conditions in spatially separated wells of a modified multi-well plate for humidity assay of plant-pathogen interactions with good throughput. We demonstrated that a discrete humidity gradient could be formed within a few minutes and maintained over a period of a few days inside the device. The device consisted of a freeway channel in the top layer, multiple compartmented wells in the bottom layer, a water source, and a drying agent source. The combinational effects of evaporation, diffusion, and convection were synergized to establish the stable discrete humidity gradient. The device was employed to study visible and molecular disease phenotypes of soybean in responses to infection by *Phytophthora sojae*, an oomycete pathogen, under a set of humidity conditions, with two near-isogenic soybean lines, Williams and Williams 82, that differ for a *Phytophthora* resistance gene (*Rps1-k*). Our result showed that at 63% relative humidity, the transcript level of the defense gene *GmPR1* was at minimum in the susceptible soybean line Williams and at maximal level in the resistant line Williams 82 following *P. sojae* CC5C infection. In addition, we investigated the effects of environmental temperature, dimensional and geometrical parameters, and other configurational factors on the ability of the device to generate miniature humidity environments. This work represents an exploratory effort to economically and efficiently manipulate humidity environments in a space-limited device and shows a great potential to facilitate humidity assay of plant seed germination and development, pathogen growth, and plant-pathogen interactions. Since the proposed device can be easily made, modified, and operated, it is believed that this present humidity manipulation technology will benefit many laboratories in the area of seed science, plant pathology, and plant-microbe biology, where humidity is an important factor that influences plant disease infection, establishment, and development. *Published by AIP Publishing.* [http://dx.doi.org/10.1063/1.4950998]

INTRODUCTION

Controlled humidity environments are highly desired in plant science and agriculture research.[1–3] The ability to generate stable and controllable humidity conditions is of significant benefit for assaying the role of air water content in seed germination and plant development

[a)]Author to whom correspondence should be addressed. Electronic mail: ldong@iastate.edu

and growth and studying interactions between plants and biological species (e.g., microbes, pathogens, and pests).[4] Current greenhouse and growth chamber technologies require sensors and computer-assisted water spray and air ventilation to obtain specified humidity levels.[5,6] Air humidity-regulating control of commercial plant growth environments is often obtained by combining humidifier and dehumidifier.[7] These methods have relatively insufficient flexibility and low accuracy in creating a large number of variable humidity levels, thus affecting throughput of various humidity assays in plant sciences. New research and development efforts of considerable magnitude are therefore needed to realize flexible, precise, and economic regulation of humidity environments with high efficiency.

Concentration gradients of diffusible molecules have been flexibly generated in microfluidic lab-chip devices using flow-based or diffusion-based methods.[8–12] These approaches allow for flexible manipulation of chemical concentrations at a small scale, thus facilitating studying many scientifically important biological phenomena, such as chemotaxis and morphogenesis of single cells and multicellular microorganisms.[13–19] The flow-based method uses an external pumping system to produce stable gradients perpendicular to parallel laminar flows of varying concentrations. The diffusion-based approach produces a chemical concentration gradient along a channel by free-diffusion between two sources, but the resulting gradient is often hard to maintain over long time periods.[20,21] Kang *et al.*[22] developed a device that generated concentration gradients parallel to the direction of flow by using a convective-diffusive balance in a counter-flow configuration. Du *et al.*[23] established spatially and temporally controllable concentration gradients of molecules in a microfluidic device. Nezhad *et al.*[24] developed diffusion based and flow based gradient microfluidic devices to stimulate pollen tubes.

While continuing efforts have been made to realize various miniature controlled environments for different biological applications, it should be pointed out that flexible manipulation of discrete humidity environments is relatively under-researched in miniaturization research and development area for plant science, plant pathology, and plant-microbe biology, where humidity is regarded as one of the major environmental factors in affecting plant disease infection, establishment, and development.

Soybean [*Glycine max* (L.) Merr.] is one of the most important crops with high economic value worldwide. In the United States, soybean is the second most important row crop after corn. It is estimated that soybean suffers yield reduction valued over 2.6 billion dollars annually from various diseases.[25] Among the diseases, *Phytophthora* root and stem rot caused by *Phytophthora sojae* alone results in annual soybean yield losses valued around 0.3 billion dollars.[26] *P. sojae* is an oomycete pathogen and can cause pre-emergence damping off leading to total crop failure. Owing to its economic importance of the disease, soybean-*P. sojae* has been widely accepted as a model plant-pathogen interaction for over four decades.

A series of *Rps* genes has been identified and utilized in breeding *Phytophthora* resistant soybean cultivars.[27] Of these, the *Rps1-k* locus was cloned. It contains two genes encoding coiled coil-nucleotide binding-leucine repeat containing proteins.[28,29] Because the oomycete pathogen *P. sojae* evolves rapidly and overcomes the newly introduced *Rps* genes,[30] a better understanding of this model system is becoming essential for designing or creating durable *Phytophthora* resistant soybean line. Furthermore, plant diseases are greatly influenced by various environmental conditions (e.g., light, temperature, soil water stress, nitrogen, etc.). Among these environmental factors, relative humidity or air water content plays a major role in disease development. Unfortunately, how the environmental humidity factor influences the outcome of the soybean-*P. sojae* interaction is unknown.

In this paper, we report on the development of a highly economical and accessible miniature device that is able to create a stable discrete humidity gradient in a space suitable for studying humidity requirements of the soybean-pathogen interaction. The proposed multi-well plate-like humidity devices can be easily made, used, and modified by unskilled persons in most biology and agriculture laboratories. We demonstrated the workability of the humidity device in assaying humidity conditions for studying both visible and molecular phenotypes in the soybean *P. sojae* interaction.

DEVICE DESIGN

The proposed device consists of two layers in a vertical direction (Figs. 1(a) and 1(d)). The top layer is spatially continuous and capped by a transparent lid. The bottom layer is partitioned into multiple identical wells. These wells are open at the top into the freeway space of the top layer. Two device configurations, namely, I-shaped and U-shaped devices, are studied for the purpose of illustrating and verifying the underlying principle. The I-shaped device has a straight top channel and a linear array of rectangular wells (Figs. 1(a)–1(c)). In the U-shaped device, an array of cylindrical wells locates in the bottom layer and a U-shaped freeway channel is formed in the top layer by using a one-end-opened partition wall (Figs. 1(d)–1(f)). To obtain a discrete humidity gradient, water and desiccant drying agent are, respectively, preloaded into two wells at the two extreme ends of the bottom layer (Figs. 1(a) and 1(d)). Water vapors evaporate from the water surface of the "source" reservoir and diffuses horizontally towards the desiccant reservoir or "drain" along the continuous top layer of the device (Figs. 1(b) and 1(e)). While passing each well, water vapors diffuse and convect downwards into the wells of the bottom layer. Herein, evaporation, diffusion, and convection are the driving forces for mass transfer of water vapors. The equilibrium concentration gradient of water vapors in the top layer arises from a balance of water evaporation at the source and water absorption by the drying agent at the drain. For each well, the water vapor right above the well serves as the source of the well, but there is no drain at the bottom of the well. As a result, when an equilibrium is established, the vapor inside the well will be distributed uniformly, except for the region near the top opening of the well where a small gradient of vapor will occur. Therefore, a steady-state discrete humidity gradient is formed within the separated wells of the bottom layer, while a continuous humidity gradient still appears in the top layer of the device (Figs. 1(c) and 1(f)). As long as the water and desiccant drying agent sources are sufficient, the discrete humidity gradient in the wells will remain in its steady state. For example, when humidity of one or multiple wells is changed due to possible absorption of water vapors by plant seeds or pathogens, the water vapors in the top freeway channel will automatically transport into the corresponding wells to compensate for the vapor loss until reaching a new equilibrium vapor gradient through local diffusion and convection.

To accommodate the size of soybean seedlings, each well in the I-shaped device was designed to be 10 mm long, 35 mm wide, and 35 mm tall. There were 12 wells in the bottom

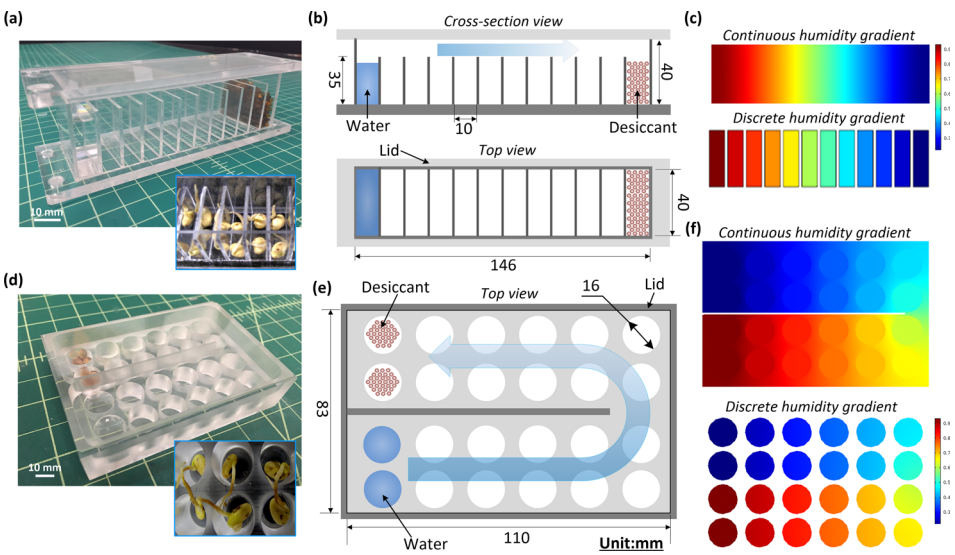

FIG. 1. Generation of a discrete humidity gradient in the I-shaped (a-c) and U-shaped (d-f) devices. Device photos are shown in (a) and (d). Schematics with key dimensions are given in (b) and (e). (c) and (f) give humidity gradients (top view) in the top and bottom layers of the I-shaped (c) and U-shaped (f) devices, respectively. Insets in (a) and (d) show soybean in the devices for studying soybean-pathogen interactions.

layer, with a 2 mm separation between the adjacent wells. The top layer of the device was comprised of 5 mm deep space between the bottom layer and the transparent slab lid (Figs. 1(a) and 1(b)). The outer dimensions of the device were 146 mm (L) × 40 mm (W) × 40 mm (H). The I-shaped device was assembled by gluing multiple pieces of pre-machined transparent poly (methyl methacrylate) or PMMA (1/8-in. thick; Plexiglas; Alsip, USA) using acrylic adhesives (3M8155; 3M; St. Paul, USA). The U-shaped device was designed to be like a commercial 24-well tissue culture plate. This device had the outer dimensions of 110 mm (L) × 83 mm (W) × 25 mm (H) and the size of each well was 16 mm diameter and 15 mm deep. The separation between the adjacent wells of this device was 2.5 mm. The top freeway channel was 8 mm in depth (Figs. 1(d) and 1(e)). The digital pattern of the U-shaped device was designed in AutoCAD (Autodesk; San Rafael, CA) and fabricated with a PMMA block (3/4-in. thick; Plexiglas; Alsip, USA) by using a high-precision milling machine (CNC Masters; Irwindale, USA).

To study dynamic process of generating a discrete humidity gradient in the I-shaped and U-shaped devices, we built a computational model for the devices, based on a finite element analysis (FEA) method based software COMSOL Multiphysics (Burlington, USA). Generally, relative humidity has a linear function with water vapour concentration in the air.[31] The FEA simulations were conducted by establishing an equilibrium relation between the vapour source, the drain with the drying agent, and the moist air concentrations at different locations of the top and bottom layers. A convection-diffusion model was thus used to simulate the humidity gradient generation process in the device based on the convection-diffusion transport equation below

$$\frac{\partial c}{\partial t} + \nabla \cdot (-D\nabla c) + u \cdot \nabla c = 0, \tag{1}$$

where c, D, and u are the concentration, the diffusivity, and the flow rate of water molecules in gaseous state, respectively. The diffusion coefficient D was set as 2.82×10^{-5} m^2/s at room temperature.[32] The flow rate of water molecules u was set at zero due to no external driving force. For normalization purpose, a constant vapour concentration of 1 mol/m^3 was used at the water reservoir and zero concentration was used at the desiccant reservoir. Time increment was set to be 5 s to illustrate the time-varying process of forming a discrete humidity gradient. A steady-state analysis was conducted to check uniformity and stability of the generated gradient.

Fig. 2(a) shows time-lapse images of the simulated humidity profiles at different time points in the I-shaped device. Fig. 2(b) shows time-varying humidity in each well of this device. The simulation result indicates the closer the well was away from the water source, the shorter the time required to establish a stable humidity in the well. Specifically, the shortest establishment time was ~130 s for the first well (see label #1 in Fig. 2(a)), while the longest time was ~550 s for the last well (see label #10 in Fig. 2(a)). Fig. 2(c) shows the steady-state humidity gradient in the I-shaped device. Five humidity-tracing lines were set at different depths of the device. The result shows that due to combining the upper freeway channel and the lower compartmented wells, a discrete humidity gradient was well established along the wells in the bottom layer, while a continuous humidity gradient appeared in the top layer and decreased along the diffusing direction (line A in Fig. 2(c)). It should be noted that the humidity of each well was spatially uniform (lines C-E in Fig. 2(c)), except for a small humidity drop at the opening of the well (line B in Fig. 2(c)). The spatial resolution of discrete gradient depends on the number of wells included in the device. For example, for the I-shaped device, let us assume the relative humidity levels above the water and desiccant reservoirs are RH_{wt} and RH_{des}, respectively, and there are N number of wells in the device. The humidity level in well n ($1 \le n \le N$) can be estimated as $(RH_{wt} - RH_{des})n/N + RH_{des}$.

Similarly, we also conducted simulations for the U-shaped device and obtained similar results as shown in Figs. 2(d)–2(f). In particular, the simulated time of reaching a stable humidity in a well varied from ~140 s at well #1 to ~820 s at well #10. It should be noted

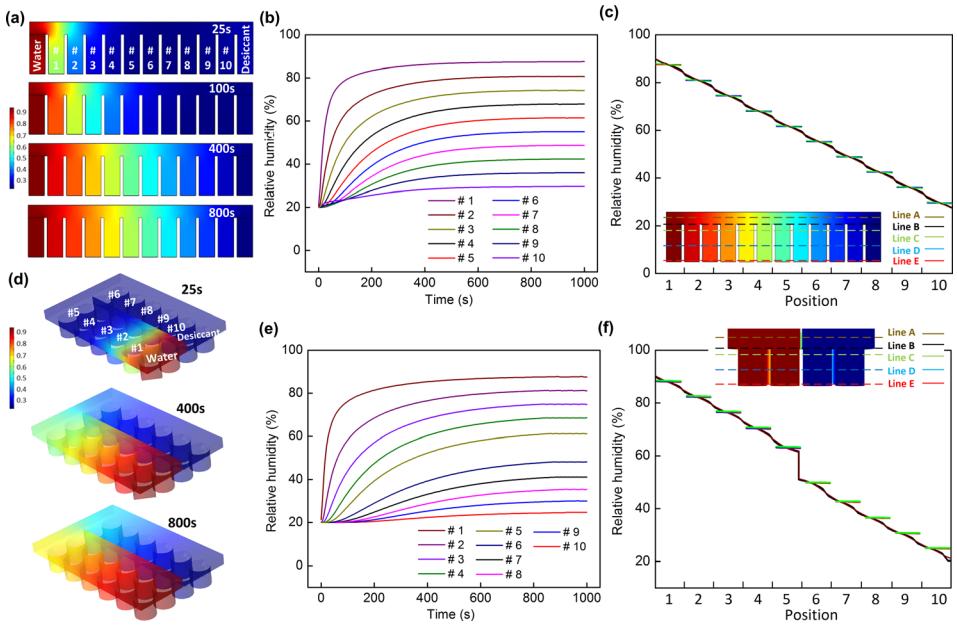

FIG. 2. Simulated dynamic process to generate discrete humidity gradients in the I-shaped and U-shaped devices. (a) and (d) give time-lapse images of water vapor movement inside the devices at different time points. (b) and (e) plot simulated relative humidity as a function of time in each well of the I-shaped (b) and U-shaped (e) devices. The wells of the I-shaped and U-shaped devices are numbered from #1 to #10 as shown in (a) and (c), respectively. The water and drying agent reservoirs are not numbered. (c) and (f) give simulated steady-state relative humidity gradient in the continuous top layer (line A), at the interface (line B) between the top and bottom layer, and at the three different depths (lines C-E) in the welled bottom layer, of the I-shaped (c) and U-shaped (f) devices, respectively.

that the humidity values of wells #5 and #6 at the spatial turning point of the U-shaped device were deviated from a linear fit for all humidity data (Fig. 2(f)). This is because the geometrical constrains of these two wells were not similar to other wells in the same device (Fig. 2(b)).

DEVICE CHARACTERIZATION

To monitor humidity development process in the wells of the lower layer of the device, we inserted four mini relative humidity sensors (SHT11; Sensirion, Staefa, Switzerland) into the wells #1, #5, #6, and #10 (at the half depth of the wells) *via* the tiny holes punched through the transparent lid. These holes were sealed witch epoxy before measurement. The relative humidity sensors were controlled by a microcontroller board (Arduino Duemilanove; Arduino LLC, Somerville, USA) to multiplex readouts. Real-time relative humidity data were collected by a built-in program of the Arduino board via a USB cable.

Fig. 3(a) shows the measured process of generating a stable discrete relative humidity gradient in the I-shaped device. The result demonstrates that depending on the location of a well, it took about 100 to 600 s to reach a steady-state humidity and that the stabilized humidity remained constant over the tested 48 h. As expected, the wells closer to the water reservoir require shorter time to establish stable humidity environments. Also, there is a close correspondence between the discrete humidity gradients generated via the FEA simulation and in the conducted experiments (Fig. 3(b)). Fig. 3(c) indicates that the wells had a decreasing relative humidity from ~91%, next to the water reservoir, to ~22%, next to the desiccant reservoir. In the U-shaped device, the measured discrete relative humidity values and distribution (Figs. 3(d)–3(f)) were similar to the simulation results mentioned. Specifically, the steady-state relative humidity levels were 90%, 82%, 76%, 69%, 63%, 48%, 44%, 37%, 29%, and 21% from well #1 to #10. The lowest relative humidity (21%) was stabilized within ~750 s, while the highest one (90%) was obtained within ~170 s.

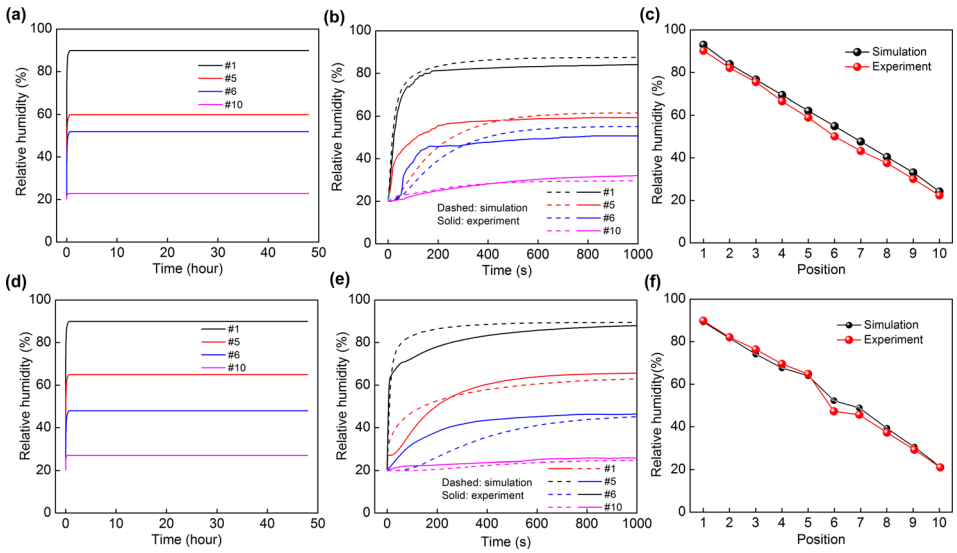

FIG. 3. Experimental humidity generation process in four wells (#1, #5, #6, and #10) of the I-shaped and U-shaped devices each, over a 48-hour period (a, d) and a close-up of the first 1000 seconds (b, e). For the purpose of comparison, the simulated results of relative humidity as a function of time are also given in (b, e). Experimental steady-state humidity in each well is given in (c, f). Here, (a-c) and (d-f) present the results for the I-shaped and U-shaped devices, respectively.

HUMIDITY IN THE SOYBEAN-*PHYTOPHTHORA SOJAE* INTERACTION

We investigated the influences of the discrete relative humidity gradient generated in the U-shaped device on visible and molecular phenotypes in the soybean-*P. sojae* interaction. Williams (*rps1-k*) is susceptible to *P. sojae* CC5C isolate, while Williams 82 is resistant due to introgression of the *Phytophthora* resistance *Rps1-k* gene into the Williams background from the soybean line Kingwa. Two-day old etiolated seedlings of the soybean cultivars Williams and Williams 82, grown in coarse vermiculites, were either inoculated with *P. sojae* isolate CC5C zoospores (1×10^5 spores/ml) or treated with sterile water and then incubated under a range of relative humidity from 21% to 90% in dark and at 22 °C for up to 48 h in the U-shaped device (Fig. 4). We observed that the development of typical disease phenotypes was depended on humidity conditions. Typical dark brown hypersensitive response (HR) was observed for Williams 82, while similar dark brown symptom response was recorded for the susceptible Williams line under lower relative humidity condition (below 45%) due to failure of the pathogen to establish compatible interactions. Seedlings of both lines shriveled when relative humidity was 21%.

To determine the role of humidity on the host responses to pathogen infection, we conducted quantitative RT-PCR (qRT-PCR) for the soybean defense gene *GmPR1*. Total RNA samples were extracted from the *P. sojae*-infected or water treated root tissues using the miRNeasy Mini Kit (Qiagen; Venlo, Limburg, the Netherlands). To eliminate any contaminating genomic DNA, we treated the RNA samples with DNase I (Promega; Madison, WI, USA) for 30 min at 37 °C. RNA samples were evaluated for quality by running on a 0.7% agarose gel and quantified by a NanoDrop ND-1000 spectrophotometer (Thermo Fisher Scientific; Waltham, MA, USA). First-strand cDNAs were synthesized from 2 μg total RNA using M-MLV reverse transcriptase (Promega; Madison, WI, USA) according to the manufacturer's recommendation. Real-time qPCR was performed on an iCycler Real-Time system (Bio-Rad; Hercules, CA, USA). Each reaction was conducted in a final volume of 20 μl containing 10 μl of iTag Universal SYBR Green (Bio-Rad; Hercules, CA, USA), 2.0 μl of cDNA sample, and 200 nM gene-specific primers. The qPCR conditions were as follows: the amplification cycles were composed of 95 °C for 30 s followed by 40 cycles of 95 °C for 15 s, 55 °C for 30 s, 72 °C for 30 s, and a final extension cycle of 72 °C for 10 min. At the end of the 40 cycles, a melting curve was generated to analyze the specificity of the reactions. Each

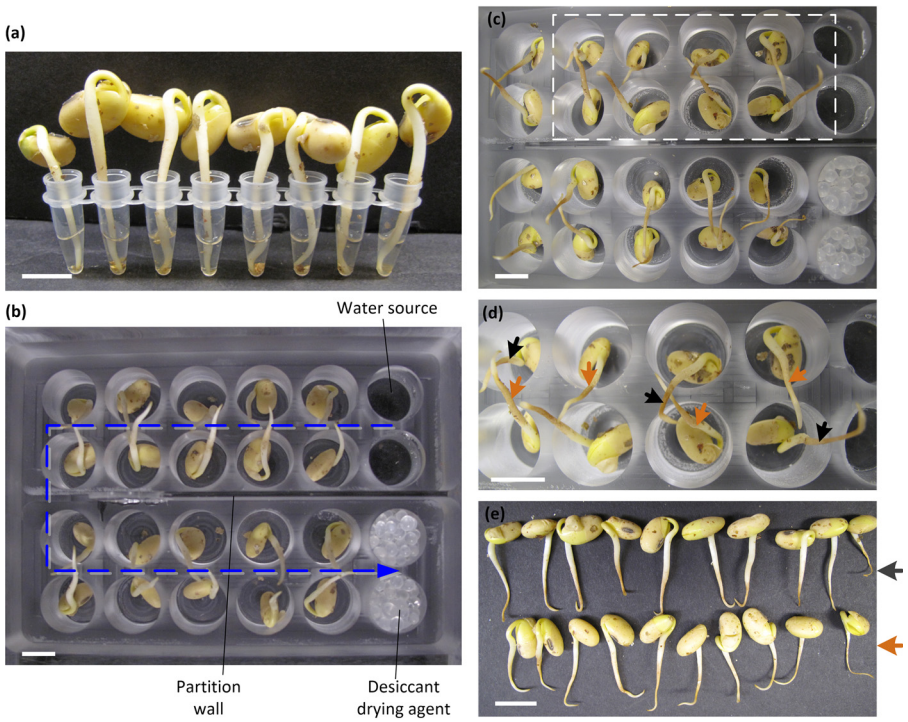

FIG. 4. Investigation of the soybean-*P. sojae* interaction under variable relative humidity conditions. A pair of near isogenic soybean lines that differ for a *Phytophthora* resistance gene (*Rps1-k*) was investigated for responses of soybean to the oomycete pathogen under a range of humidity conditions. Two-day old etiolated soybean seedlings of the cultivar Williams (*rps1-k*) and Williams 82 (*Rps1-k*) were inoculated with 100 μl *P. sojae* isolate CC5C zoospores suspension (10^5 spores/ml) for 30 min as shown in (a). A range of humidity condition was generated by the U-shaped device shown in Fig. 1(c). Inoculated seedlings were arranged upside down in the device as shown in (b). Twenty-four hours following inoculation, the seedlings were observed for disease phenotypes (c) and (d). The seedlings shown in (d) are from the zoomed section of (c), shown by a white rectangle. In (d), black arrows show the resistant response of Williams 82 (*Rps1-k*) to the pathogen, while orange arrows show the susceptible response of Williams (lacking *Rps1-k*) to the pathogen. In (e), ten *P. sojae* infected seedlings under variable humidity condition are shown. The black arrows show resistant response of Williams 82 (upper panel) and the orange arrows indicate susceptible response of Williams (lower panel) under variable relative humidity condition with the left most seedlings were exposed to 90% relative humidity while the right most ones to 21% relative humidity. Scale bars in (a)-(e) represent 10 mm.

cDNA sample was PCR amplified in three replications. The ELF1B transcript level was used as the endogenous control. The relative expression level was calculated as $2^{-\Delta\Delta CT}$ ($\Delta CT = CT$, gene of interest — CT, ELF1B. $\Delta\Delta CT = \Delta CT$, treatment — ΔCT, 21% relative humidity control). Fig. 5 shows relative expression of the soybean defense *GmPR1* gene in the roots of etiolated soybean seedlings either treated with water or infected with *P. sojae* under different humidity conditions. It is expected that in a typical susceptible host response, the *GmPR1* levels will be at minimal level. On the other hand, the *GmPR1* level will be at maximum level in a typical resistant response governed by recognition of an *Rps* gene product by its corresponding *Avr* effector protein encoded by an *Avr* gene. The result of the humidity assay shown in Fig. 5 indicates that at 63% relative humidity, the *GmPR1* transcripts are at the minimal level in the infected roots of the susceptible line, Williams, and at the maximal level in the infected roots of the resistant line, Williams 82. Therefore, this study indicates that for a successful soybean-*P. sojae* interaction, the relative humidity should be around 63%. We also, however, observed that at low relative humidity (e.g., 44%, Fig. 5(a)), the susceptible line Williams showed enhanced expression of the *GmPR1* gene because under low humidity condition the pathogen fails to infect the host normally and host gets the upper-hand to fight back by inducing defense pathway and induction of HR response (Fig. 4), presumably triggered by pathogen-associated molecular patterns (PAMPs).

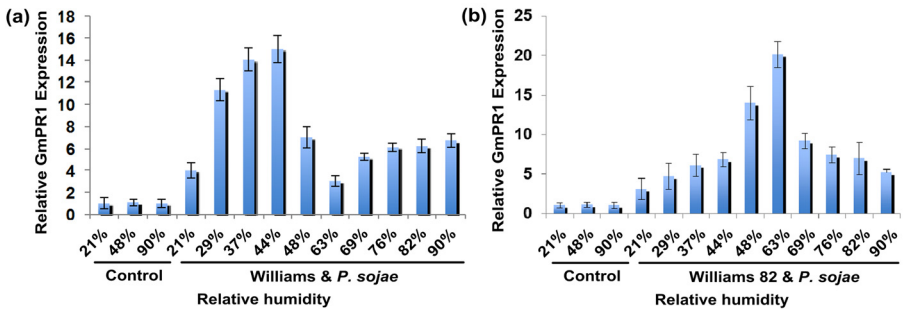

FIG. 5. Relative expression of soybean defense *GmPR1* gene in infected roots of etiolated soybean seedlings with *P. sojae* under different humidity conditions as compared to that in the control. (a) Phenotypes of the susceptible and resistant host responses of Williams and Williams 82, respectively, to *P. sojae* isolate CC5C. (a) Expression of the defense gene *GmPR1* in Williams. Control, seedlings treated with water; Williams and *P. sojae*, compatible interaction or susceptible host response following infection of Williams with *P. sojae*. (b) Expression of the defense gene *GmPR1* in Williams 82. Control, seedlings treated with water; Williams 82 and *P. sojae*, incompatible interaction or resistant host response following infection of Williams 82 with *P. sojae*. Histograms show the mean of three biological replications and bars indicate standard errors calculated from standard deviations of three independent biological replications.

TEMPERATURE, SIZE SCALING, AND OTHER CONFIGURATIONS

While the utility of the U-shaped device for determining humidity requirements of the soybean-*P. sojae* interaction has been demonstrated, it is also worth studying the effects of environmental temperature and dimensional and geometrical parameters on the device performance in order to further explore other possible applications in the future.

We first studied how environmental temperature influences the formation of discrete humidity gradient within the I-shaped and U-shaped devices. In this experiment, each device was placed on a digital hotplate and a temperature and humidity sensor was inserted into well #6 of the device (Figs. 1(a) and 1(d)). The result shows that as the temperature increases from 22 °C to 50 °C, the steady-state humidity of the well decreased from ∼52% to ∼28% (Figs. 6(a) and 6(c)). Note that relative humidity is defined as the ratio of the partial pressure of water vapour to the equilibrium vapour pressure of water at a temperature. The equilibrium vapour pressure of water vapour increased fast as temperature rose, while the partial pressure of water vapour was little influenced by temperature. As a result, the steady-state humidity decreased with increasing temperature (Figs. 6(b) and 6(d)).

To accommodate for smaller seeds (e.g., *Arabidopsis*, rice, etc.) for future research, we also studied the effect of device size on humidity generation of the device. We applied different scaling factors (SF = 1.0, 0.7, 0.5, 0.25, 0.125, 0.1, and 0.05) to the original dimensions of the U-shaped device (Figs. 1(d) and 1(e)). The simulation result shows that the time required to reach a stable humidity level reduced with decreasing device size (Fig. 7(a)). We then manufactured a smaller U-shaped device with the dimensions of 77 mm × 58.1 mm × 17.5 mm (SF = 0.7) to house 24 wells with each being 11.2 mm diameter and 10.5 mm deep. A humidity generation and measurement experiment was also taken on the device, where one end was set as the water source and the other was set as the drying agent source. A thin layer (∼1 mm thick) of desiccant powders was laid at the bottom of each well to indicate humidity difference between the wells. At low humidity levels, the color of the desiccant powders was yellow. As the humidity increased, the desiccant powders became slightly blue. Fig. 7(b) indicates that a stable discrete humidity gradient was established within 6.5 min, almost matching the simulated result (green curve in Fig. 7(a)). We also made a smaller I-shaped device with the dimensions of 44 mm × 32 mm × 6 mm (see the lower panel in Fig. 7(b)). The color change of the desiccant powders indicates that the downscaled I-shaped device had a shorter establishment time of ∼1 min (Fig. 7(b)). Furthermore, it should be noted that as long as water and drying agents in the reservoirs are adequate to consume, the boundary conditions of the aforementioned convection-diffusion equation governing the process of forming humidity gradient will not change with different reservoir sizes. Thus, the stabilized humidity gradient will not be influenced by the dimensions of the

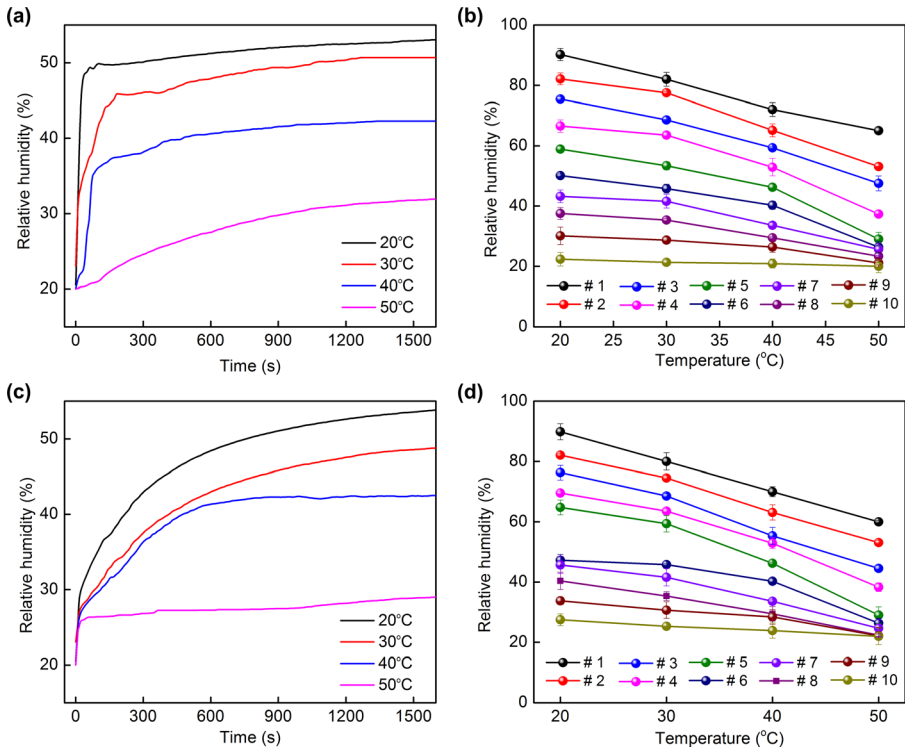

FIG. 6. Temperature effect on humidity generation process in a well of the I-shaped (a) and U-shaped (c) device. Steady-state relative humidity as a function of temperature for in all wells of the I-shaped and U-shaped devices is given in (b) and (d), respectively.

reservoirs. In addition, the gradient stabilization time is mainly determined by the distance between the water and desiccant reservoirs and not by the dimensions of the reservoirs either. Therefore, the present method of generating discrete humidity is not limited to the specific dimensions shown above but rather common in different dimensional settings.

Furthermore, by setting up the water and desiccant drying agent sources at different wells of the device, it was possible to flexibly manipulate spatial distributions of discrete humidity within the device. For example, when two desiccant sources located at two extreme ends and one water source located in the middle of the I-shaped device, a terrace-step like distribution of

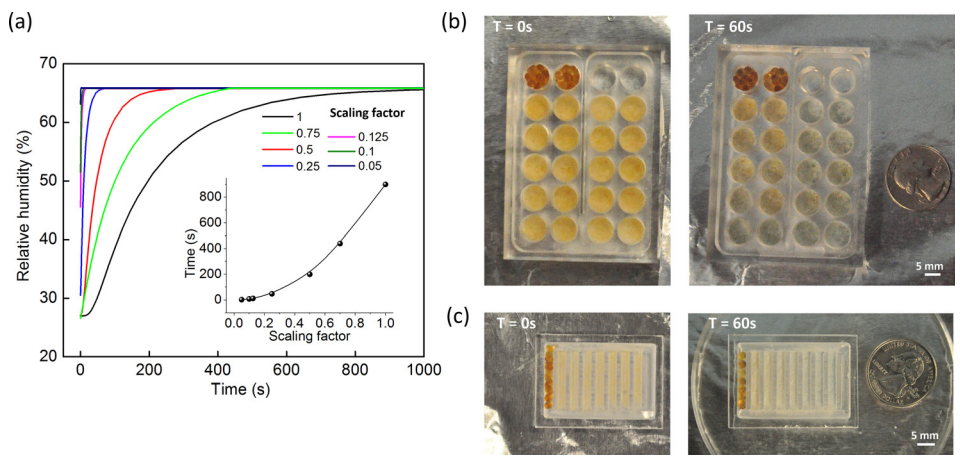

FIG. 7. (a) Influence of device size on dynamic humidity generation process of U-shaped device. Inset shows the stabilization time as a function of scaling factor. (b, c) Color change of a thin layer of desiccant powders laid at the bottom of the wells due to different humidity levels of the wells of the downscaled devices.

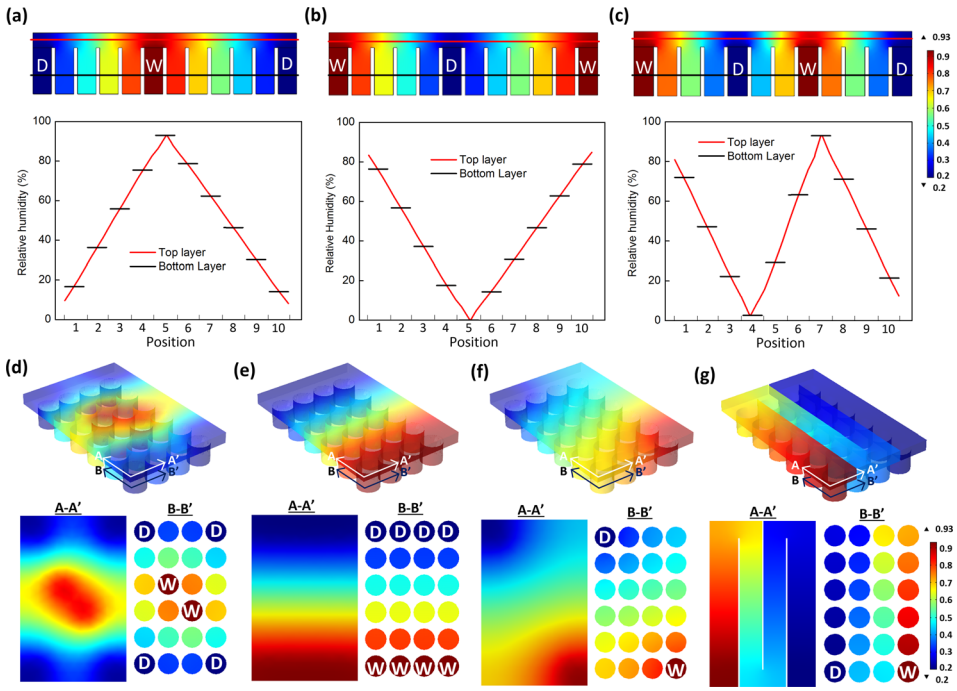

FIG. 8. Spatial manipulation of humidity distributions by setting up water and desiccant sources and partition walls at different locations in the I-shaped and U-shaped devices. The letters "D" and "W" represent desiccant and water sources, respectively. In (a)-(c), the plots in the lower row track humidity along the red and black lines in the top and bottom layers, respectively. In (d)-(f), the lower row shows distributions of humidity in the two planes (A-A′ in the top layer and B-B′ in the bottom layer) labelled on each device.

humidity was obtained with the highest level in the middle and the lowest (highest) one at the ends (Fig. 8(a)). In addition, arranging two sets of water and desiccant sources in the I-shaped device as shown in Fig. 8(c) led to a triangular wave-like distribution of humidity superimposed with a step-like modulation. Furthermore, by placing the water and desiccant sources in the center, edge, and/or corner of the device without any partition walls, the humidity distribution within the device could be well defined and predictable. Figs. 8(d)–8(f) show the discrete humidity gradients generated in three different cases, including (i) that water was loaded in the two wells near the center and the desiccant particles were loaded to the wells in four corners, (ii) that the water and desiccant particles were, respectively, loaded to the wells near the two short-length edges of the device, and (iii) that the water and desiccant particles were located at the wells in the two diagonal corners. In addition, Fig. 8(g) shows that by setting up three partition walls in the top layer of the U-type device, a serpentine top freeway channel was formed, along which a discrete humidity gradient could be established.

CONCLUSIONS

We have demonstrated a simple and effective new method to obtain a controlled discrete humidity gradient in miniature multi-plate like devices. The device was composed of a freeway channel in the top layer, multiple compartmented wells in the bottom layer, a water source, and a desiccant source. A stable discrete humidity gradient was generated within up to a few minutes and maintained via the combinatory effects of evaporation, convection, and diffusion of water vapors inside the device. We have also demonstrated the workability of the device in studying the soybean *P. sojae* interaction at various humidity conditions. Based on the visible and molecular phenotypes of soybean in responses to *P. sojae*, we came to the conclusion that 63% relative humidity is the most suitable for generating compatible and incompatible interactions in this plant-pathogen interaction.

The present humidity generation method provides sufficient flexibility in manipulating spatial distribution of stable discrete humidity gradient inside a miniature device. This approach can be readily translated into smaller scale devices to accommodate smaller plant species, such as *Arabidopsis thaliana*.[33] By considering the low cost and ease of fabrication, use, and modification of the device, this method represents a valuable platform for air humidity assay of plant seed germination and development, pathogen growth, and plant-pathogen interaction. In addition, the present device should be useful for many other biological processes where relatively rapid generation and long-term stabilization of discrete air humidity gradient are needed. We believe that the present technology will benefit many research areas including plant science, plant pathology, plant-microbe interaction, and agronomy in general.

Future work includes introduction of additional economic control mechanisms for adjusting other environmental parameters such as light and temperature in the present device.[34,35] Such a modified humidity device will be a very powerful platform to conduct biological assays for determining role of various environmental factors in plant-pathogen, plant-microbe interactions, and also in studying seed germination and plant development.

ACKNOWLEDGMENTS

This work was supported in part by the U.S. National Science Foundation under Grant No. DBI-1331390 to L.D., United States Department of Agriculture's National Institute of Food and Agriculture program under Grant No. 2013-68004-20374 to L.D. and M.K.B., Iowa Corn Promotion Board, Iowa State University's Plant Sciences Institute Faculty Scholar program to L.D. and M.K.B, and China Scholarship Council to H. J.

[1]J. L. Shipp, Y. Zhang, D. W. A. Hunt, and G. Ferguson, Environ. Entomol. **32**(5), 1154–1163 (2003).
[2]P. B. Reich and R. G. Amundson, Science **230**(4725), 566–570 (1985).
[3]K. A. Mott and D. F. Parkhurst, Plant Cell Environ. **14**(5), 509–515 (1991).
[4]D. J. Hannusch and G. J. Boland, Eur. J. Plant Pathol. **102**(2), 133–142 (1996).
[5]K. O. Korner and H. Challa, Comput. Electron. Agric. **39**(3), 173–192 (2003).
[6]K O. Korner and H. Challa, Comput. Electron. Agric. **43**(1), 1–21 (2004).
[7]J. S. Perret, A. M. Al-Ismaili, and S. S. Sablani, Biosyst. Eng. **91**(3), 349–359 (2005).
[8]T. M. Keenan and A. Folch, Lab Chip **8**(1), 34–57 (2008).
[9]S. K. W. Dertinger, D. T. Chiu, N. L. Jeon, and G. M. Whitesides, Anal. Chem. **73**(6), 1240–1246 (2001).
[10]M. A. Holden, S. Kumar, E. T. Castellana, A. Beskok, and P. S. Cremer, Sens. Actuators, B **92**(1–2), 199–207 (2003).
[11]R. F. Ismagilov, A. D. Stroock, P. J. A. Kenis, G. Whitesides, and H. A. Stone, Appl. Phys. Lett. **76**(17), 2376–2378 (2000).
[12]B. R. Gorman and J. P. Wikswo, Microfluid. Nanofluid. **4**(4), 273–285 (2008).
[13]N. L. Jeon, H. Baskaran, S. K. W. Dertinger, G. M. Whitesides, L. Van de Water, and M. Toner, Nat. Biotechnol. **20**(8), 826–830 (2002).
[14]A. Khademhosseini, R. Langer, J. Borenstein, and J. P. Vacanti, Proc. Natl. Acad. Sci. U.S.A. **103**(8), 2480–2487 (2006).
[15]A. Shamloo, N. Ma, M.-m. Poo, L. L. Sohn, and S. C. Heilshorn, Lab Chip. **8**(8), 1292–1299 (2008).
[16]B. G. Chung, L. A. Flanagan, S. W. Rhee, P. H. Schwartz, A. P. Lee, E. S. Monuki, and N. L. Jeon, Lab Chip **5**(4), 401–406 (2005).
[17]J. Pihl, J. Sinclair, E. Sahlin, M. Karlsson, F. Petterson, J. Olofsson, and O. Orwar, Anal. Chem. **77**(13), 3897–3903 (2005).
[18]B. G. Chung, F. Lin, and N. L. Jeon, Lab Chip **6**(6), 764–768 (2006).
[19]M. S. Yang, J. Yang, C. W. Li, and J. L. Zhao, Lab Chip **2**(3), 158–163 (2002).
[20]B. Mosadegh, C. Huang, J. W. Park, H. S. Shin, B. G. Chung, S.-K. Hwang, K.-H. Lee, H. J. Kim, J. Brody, and N. L. Jeon, Langmuir **23**(22), 10910–10912 (2007).
[21]V. V. Abhyankar, M. A. Lokuta, A. Huttenlocher, and D. J. Beebe, Lab Chip **6**(3), 389–393 (2006).
[22]T. Kang, J. Han, and K. S. Lee, Lab Chip **8**(7), 1220–1222 (2008).
[23]Y. Du, J. Shim, M. Vidula, M. J. Hancock, E. Lo, B. G. Chung, J. T. Borenstein, M. Khabiry, D. M. Cropek, and A. Khademhosseini, Lab Chip **9**(6), 761–767 (2009).
[24]A. S. Nezhad, M. Packirisamy, and A. Geitmann, Plant J. **80**(1), 185–195 (2014).
[25]J. A. Wrather and S. R. Koenning, J. Nematol. **38**(2), 173–180 (2006).
[26]D. Sandhu, H. Y. Gao, S. Cianzio, and M. K. Bhattacharyya, Genetics **168**(4), 2157–2167 (2004).
[27]D. Sandhu, K. G. Schallock, N. Rivera-Velez, P. Lundeen, S. Cianzio, and M. K. Bhattacharyya, J. Heredity **96**(5), 536–541 (2005).
[28]H. Y. Gao, N. N. Narayanan, L. Ellison, and M. K. Hattacharyya, Mol. Plant-Microbe Interact. **18**(10), 1035–1045 (2005).
[29]H. Gao and M. K. Bhattacharyya, BMC Plant Biol. **8**(1), 1 (2008).

[30]A. F. Schmitthenner, M. Hobe, and R. G. Bhat, Plant Disease **78**(3), 269–276 (1994).
[31]A. Laugier and J. Garai, J. Chem. Educ. **84**, 1832 (2007).
[32]J. S. Rowlinson, Chem. Br. **20**(11), 1027–1027 (1984).
[33]S. Kaul *et al*. Nature **408**(6814), 796–815 (2000).
[34]H. Jiang, Z. Xu, M. R. Aluru, and L. Dong, Lab Chip **14**(7), 1281–1293 (2014).
[35]H. Jiang, Y. Jiao, M. R. Aluru, and L. Dong, J. Nanosci. Nanotechnol. **12**(8), 6333–6339 (2012).